ACS Catalysis

Research Article

pubs.acs.org/acscatalysis

Wafer-Level Artificial Photosynthesis for CO_2 Reduction into CH_4 and CO Using GaN Nanowires

Bandar AlOtaibi,[†] Shizhao Fan,[†] Defa Wang,[‡,§] Jinhua Ye,[‡,∥] and Zetian Mi*[,†]

[†]Department of Electrical and Computer Engineering, McGill University, 3480 University Street, Montreal, Quebec H3A 0E9, Canada

[‡]TU-NIMS Joint Research Center, School of Materials Science and Engineering, Tianjin University, 92 Weijin Road, Nankai District, Tianjin 300072, China

[§]Collaborative Innovation Center of Chemical Science and Engineering (Tianjin), 92 Weijin Road, Nankai District, Tianjin 300072, China

[∥]International Center for Materials Nanoarchitectonics (WPI-MANA) and Environmental Remediation Materials Unit, National Institute for Materials Science (NIMS), 1-1 Namiki, Tsukuba, Ibaraki 305-0044 Japan

Supporting Information

ABSTRACT: We report on the first demonstration of high-conversion-rate photochemical reduction of carbon dioxide (CO_2) on gallium nitride (GaN) nanowire arrays into methane (CH_4) and carbon monoxide (CO). It was observed that the reduction of CO_2 to CO dominates on as-grown GaN nanowires under ultraviolet light irradiation. However, the production of CH_4 is significantly increased by using the Rh/Cr_2O_3 core/shell cocatalyst, with an average rate of ~3.5 μmol g_{cat}^{-1} h^{-1} in 24 h. In this process, the rate of CO_2 to CO conversion is suppressed by nearly an order of magnitude. The rate of photoreduction of CO_2 to CH_4 can be further enhanced and can reach ~14.8 μmol g_{cat}^{-1} h^{-1} by promoting Pt nanoparticles on the lateral *m*-plane surfaces of GaN nanowires, which is nearly an order of magnitude higher than that measured on as-grown GaN nanowire arrays. This work establishes the potential use of metal-nitride nanowire arrays as a highly efficient photocatalyst for the direct photoreduction of CO_2 into chemical fuels. It also reveals the potential of engineered core/shell cocatalysts in improving the selectivity toward more valuable fuels.

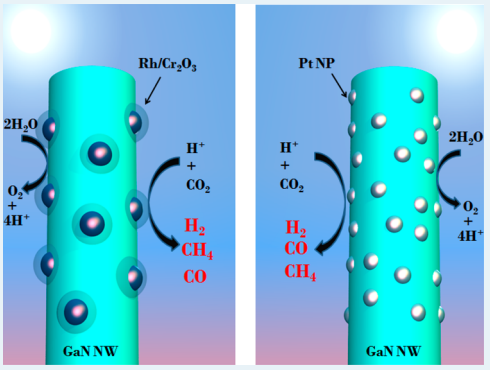

KEYWORDS: *carbon dioxide photoreduction, artificial photosynthesis, solar fuels, methane, gallium nitride, nanowires*

It has been envisioned that the chemical transformation of carbon dioxide (CO_2) may provide a promising solution to simultaneously address some of the grand challenges we face, including energy storage, energy resource shortage, as well as the negative environmental impact of the increasing greenhouse gas emissions.[1−4] In this regard, the photocatalytic reduction of CO_2 using solar energy, among other approaches, has drawn considerable attention.[5−12] Unlike the photoelectrochemical CO_2 reduction approach, the photocatalytic route generally involves only the use of CO_2, sunlight, and water without any external electrical bias. This process mimics the biological photosynthesis in plants. Light is absorbed by the semiconductor photocatalyst, and the photogenerated energetic electrons can reduce CO_2 to compounds of high standard enthalpy of combustion. Various semiconductor photocatalysts, including metal oxide, oxynitride, sulfide, and phosphide have been investigated over the last few decades.[8,9] However, molecular CO_2 has a very low electron affinity and is chemically inert and very stable. The electrochemical potential for CO_2 single-electron reduction is ∼ −1.9 V vs NHE.[13] The thermodynamic barrier for CO_2 photoreduction is relatively high for the photoexcited electrons due to the large affinity of most semiconductor photocatalysts, thereby limiting the efficiency of CO_2 conversion. Moreover, depending on the mechanism of transferring the energetic electrons, the reduction of CO_2 may follow different pathways, leading to multiple products when a single material catalyst is used. Consequently, the overall efficiency of the CO_2 photocatalytic reduction may ultimately be limited by the complexity involved in the practical separation of products. The achievement of efficient and selective production of highly valuable fuel compounds is critical for viable CO_2 photoreduction systems.

The conduction band minimum (CBM) of GaN is more negative than those of most metal oxides, and hence GaN is kinetically more probable for the reduction of highly stable CO_2 molecules.[14−17] Moreover, it can meet the thermodynamic requirements to reduce CO_2 to CO and hydrocarbons in a large range of pH solutions.[18,19] III-nitride materials have also shown

Received: February 11, 2015
Revised: July 29, 2015
Published: July 30, 2015

DOI: 10.1021/acscatal.5b00776
ACS Catal. 2015, 5, 5342−5348

excellent stability in aqueous solution.[20−22] Recent studies have further demonstrated that nonpolar metal-nitride surfaces are extremely reactive for producing H_2 directly from water under UV and visible light illumination,[22−30] which is essentially required for the hydrogenation of CO_2. The use of nanowires can further enhance the efficiency due to the drastically reduced defect densities, increased reaction sites, and superior charge carrier transfer properties at the semiconductor/electrolyte interface.

In this work, we have demonstrated, for the first time, photochemical reduction of CO_2 to CH_4 and CO on GaN nanowire arrays. It was observed that the reduction of CO_2 to CO dominates on as-grown GaN nanowires under ultraviolet light irradiation. With the use of Rh/Cr_2O_3 core/shell cocatalyst, however, the production of CH_4 is significantly increased, with an average rate of ~3.5 μmol g_{cat}^{-1} h^{-1} in 24 h, and the rate of CO_2 to CO conversion is suppressed by nearly an order of magnitude. The rate of photoreduction to CH_4 can be further enhanced and can reach ~14.8 μmol g_{cat}^{-1} h^{-1} by promoting Pt nanoparticles on the lateral *m*-plane surfaces of GaN nanowires, which is nearly 1 order of magnitude higher than that measured on as-grown GaN nanowire arrays. Compared to conventional powders, such wafer-level nanostructured semiconductors can effectively promote the solid−gas CO_2 reduction.[31−33]

RESULTS AND DISCUSSION

In this experiment, catalyst-free GaN nanowire arrays were grown directly on *n*-type Si(111) substrate by radio frequency plasma-assisted molecular beam epitaxy under nitrogen-rich conditions. The detailed growth conditions were described elsewhere.[34] The scanning electron microscopy image of GaN nanowires grown on Si is shown in Figure 1a. The wire diameters are in the range of 80 to 120 nm with lengths in the range 800 to 900 nm. The nanowires are vertically aligned on Si substrate with their sidewalls being nonpolar *m*-plane. Previous studies have shown that the Fermi level is unpinned on clean GaN surfaces.[35] The presence of negligible surface states in the midbandgap is attributed to the strong ionic characteristic of GaN where the electrostatic energy contributing to the binding energy between atoms at the surface is nearly equivalent to that in the bulk, thereby leading to the bunching of surface states close to the bandedges rather than the midbandgap.[35,36] The absence of polarization on the *m*-plane can further reduce the interface states introduced by spontaneous polarization.[37] In addition, compared to conventional planar structures grown on lattice mismatched substrates, III-nitride nanowires grown on foreign substrates are largely free of dislocations due to the effective lateral stress relaxation and the absence of an epitaxial relationship between the nanowires and the underlying substrate.[38] This leads to significantly reduced nonradiative recombination. These attributes have been previously studied.[39−41] The incorporation of metal particles on the GaN surface can significantly reduce the upward band bending of unintentionally[42,43] *n*-type doped GaN[44,45] due to the neighboring inhomogeneous Schottky's barriers.[46] That is, electrons experience less opposing electrical field, thereby leading to more efficient electron transfer. Previous studies have shown that such nanowire arrays are highly reactive for water splitting and H_2 generation.[47−49] The electrochemical potentials for the reduction of CO_2 to CH_4 and CO are schematically shown in Figure 1b. The energy band gap of III-nitrides (AlGaInN) can be varied from ~6.2 to 0.65 eV. It is interesting

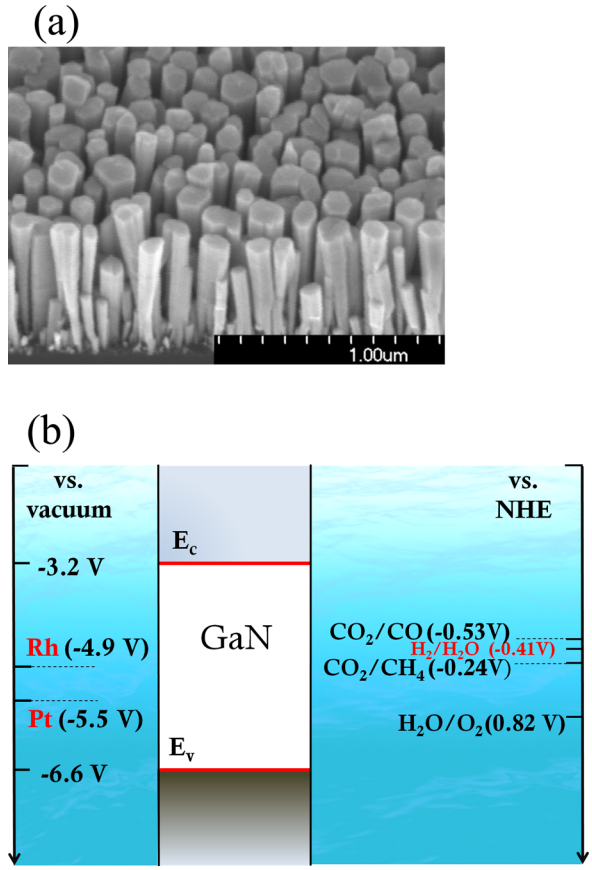

Figure 1. (a) A 45 °C tilted scanning electron microscope image of GaN nanowires grown on Si(111) substrate. (b) Band edge positions of GaN in comparison with the work function of Rh and Pt with respect to the vacuum energy level. Also shown are the CO_2/CO and CO_2/CH_4 reduction potentials versus NHE for pH = 7.

to notice that photoexcited electrons in the conduction band of GaN can be transferred to adsorbed CO_2 molecules to drive various reductive half reactions, which potentially leads to very poor product selectivity.

It has been recognized that cocatalysts such as transition metals play an important role in enhancing the efficiency and product selectivity for CO_2 photoreduction.[50−53] Transition-metal nanoparticles can form Schottky contact with GaN. The surface charge properties, including band bending, can therefore be engineered by incorporating metal nanoparticles with different work functions on the nanowire surfaces.[35,54] Among the various nanoparticle cocatalysts, Rh and Pt have work functions of ~5 and 5.5 eV, respectively, which are positioned in the fundamental energy bandgap of GaN. The larger work function of Pt may be responsible for more facile photoexcited electron transfer from the GaN nanowire, and thus, a higher reaction rate could be expected from Pt if the diffusion of electrons to nanoparticles is the rate-determining step. In addition to the enhanced charge separation and extraction, the cocatalyst metal particles can further reduce the active energy barrier of CO_2 reduction.[53,55,56] Water is commonly used as an atomic hydrogen donor for CO_2 reduction. In this regard, GaN was previously reported as an excellent photocatalyst for water oxidation.[29,30,57,58] The anion radical $CO_2^{\bullet-}$ has been first demonstrated to form on rhodium (Rh) catalysts,[56] which is essential for CO_2 to CO reduction. High activity was also shown by promoting Rh catalysts.

DOI: 10.1021/acscatal.5b00776
ACS Catal. 2015, 5, 5342−5348

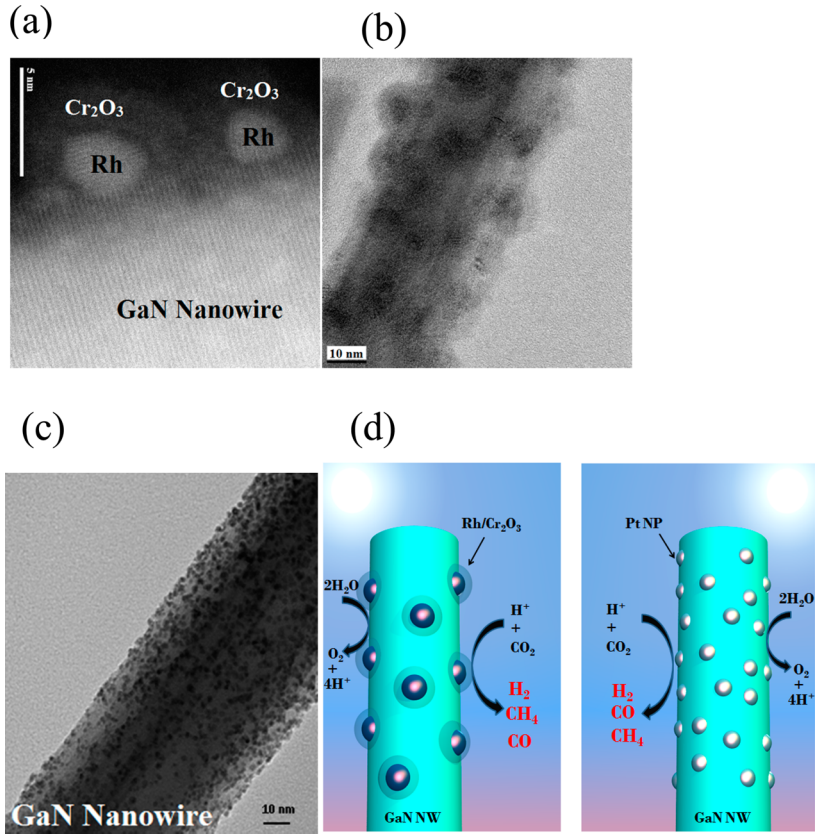

Figure 2. (a) High-resolution transmission electron microscope (TEM) image and (b) TEM image of Rh/Cr_2O_3 core/shell decorated GaN nanowire. (c) TEM image of Pt nanoparticles deposited on GaN nanowire. (d) Schematic of the photoreduction processes of CO_2 on Rh/Cr_2O_3 and Pt-decorated GaN nanowires.

Therefore, we have investigated the use of Rh nanoparticles as a promoter for hydrogenation of CO_2 to CH_4 instead of the thermodynamically unfavorable one-electron reduction of CO_2. However, we found that promoting only Rh particles on the surface of GaN nanowires did not improve CO_2 photoreduction into neither CO nor CH_4 (Supporting Information S2). Because the H_2O reforming rate is faster than that of CO_2,[59,60] the hydrogenation of CO_2 into hydrocarbons may be significantly suppressed. Therefore, an amorphous-like Cr_2O_3 shell capsuling Rh particle is utilized as O_2 molecular diffusion barrier preventing the onsite backward formation of H_2O. In this regard, the Rh metal−core nanoparticle enhances the forward reaction of CO_2 and H_2O reduction, whereas the Cr_2O_3 amorphous-shell (i) suppresses the high rate backward reaction to form H_2O from H_2 and O_2[61] and (ii) acts as an efficient CO_2 adsorption sites.[62] This noble metal on a metal-oxide support was realized earlier to be beneficial in CO_2 reduction.[60,63] A similar view is adopted for Pt nanoparticles on GaN nanowires. The configuration of the chemisorbed CO_2 on Pt is favorable for hydrogenation.[64]

High-resolution transmission electron microscopy (TEM) was used to characterize the Rh/Cr_2O_3 core/shell nanostructures photodeposited on the GaN nanowires. Figure 2a illustrates a high-resolution TEM image of Rh/Cr_2O_3 nanoparticles photodeposited on GaN nanowires. It is clearly shown that Rh/Cr_2O_3 nanoparticles were deposited on the lateral surfaces of GaN nanowires. The high-angle annular-dark-field image shown in Figure 2b confirms the uniform deposition of Rh/Cr_2O_3 core/shell nanostructures on GaN nanowires. It is observed that the GaN nanowire is single crystalline and free of structural defects. The single crystallinity and absence of structural defects have also been observed in our previous studies.[29,49] For the Rh/Cr_2O_3 core/shell structure, the metallic Rh core is well crystallized, with an average diameter of ∼3 nm, while the Cr_2O_3 shell is amorphous. The low magnification TEM image of Pt nanoparticles on GaN nanowire surface is shown in Figure 2c. The diameters of Pt nanoparticles are 1−2 nm. The TEM image shows well-distributed Pt nanoparticles along a GaN nanowire. The photoreduction processes of CO_2 on Rh/Cr_2O_3 and Pt decorated GaN nanowires are schematically shown in Figure 2d.

We have first performed CO_2 photoreduction experiments on as-grown GaN nanowire array as well as GaN nanowires with the presence of Rh/Cr_2O_3 nanoparticles. For both samples, the major products observed were H_2, CO, and CH_4. Figure 3a shows the measured CH_4 evolution over 24 h for both samples. It is seen that the rate of CH_4 formation increased from 1.3 μmol g_{cat}^{-1} h^{-1} on as-grown GaN nanowires to 3.5 μmol g_{cat}^{-1} h^{-1} on GaN decorated by Rh/Cr_2O_3 nanoparticles. This enhancement could be attributed to the effective adsorption and hydrogenation of CO_2 molecules on Rh/Cr_2O_3. Shown in Figure 3b is the measured CO evolution over 24 h for both samples. It is seen that a significant amount of CO, ∼1130 μmol g_{cat}^{-1}, was measured from the as-grown GaN nanowires in 24 h, while a drastically reduced amount of CO, ∼120 μmol g_{cat}^{-1}, was measured on Rh/Cr_2O_3-decorated GaN nanowires. It is clearly seen that promoting Rh/Cr_2O_3 nanoparticles on GaN increases the product selectivity of CH_4 over CO. That is, the conversion rate of CO_2 into CO, which is a two-electron reduction process, is suppressed by 1 order of

DOI: 10.1021/acscatal.5b00776
ACS Catal. 2015, 5, 5342−5348

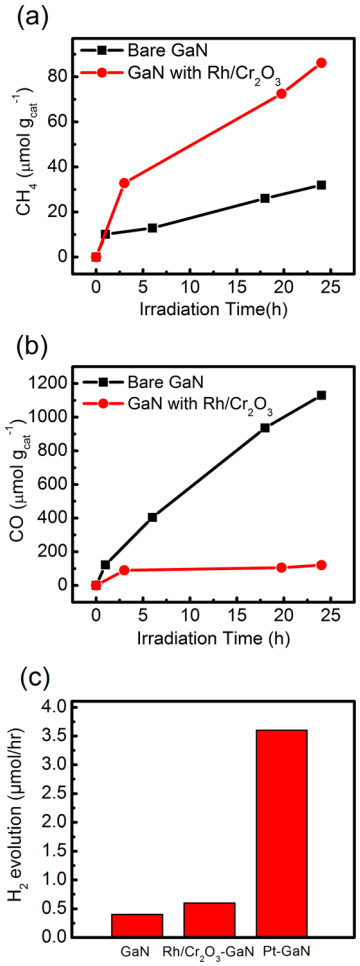

Figure 3. (a) CH_4 and (b) CO production on as-grown GaN nanowires and Rh/Cr_2O_3 decorated GaN nanowires as a function of illumination time. (c) Measured H_2 evolution rate on as-grown GaN nanowires (~8 μmol of GaN) and Rh/Cr_2O_3 and Pt-decorated GaN nanowires.

magnitude, while the production of CH_4, which is an eight-electron reduction process, has been increased by 3-fold. Also seen in Figure 3b, the CO evolution on Rh/Cr_2O_3-decorated nanowires has been inhibited after the first 2 h, implying that the photoexcited electrons are effectively collected by Rh/Cr_2O_3 core/shell nanoparticles, with no apparent reductive reaction occurring on the active sites of the exposed nanowire lateral surfaces without Rh coverage. Shown in Figure 3c is the H_2 evolution rate during these photochemical CO_2 reduction experiments (Supporting Information S1). The high H_2 formation is due the favorable simple two-electron reduction of H^+ formed from the oxidation process of water. The measured photocatalytic activities over 24 h suggest that water, rather than GaN, was being oxidized (Supporting Information S3). This is further confirmed by detailed X-ray photoelectron spectroscopy studies that showed the presence of GaN surfaces after the reaction (Supporting Information S3).

While it has been incomprehensibly observed the reduction of CO_2 toward either CH_4 or CO on rhodium,[65,66] previous studies have shown that the adsorption of CO_2 molecule on Cr_2O_3 can lead to the transformation to surface carbonate species.[62,67] The carbonate species can undergo reduction reactions to CH_4 on metal-containing oxide in the presence of protons.[68−70] In this case, the adsorbed CO can be an intermediate determining step toward CH_4 production.[68] Another pathway, which is likely to occur when H_2 is promoted, is that formate ions are formed by CO_2 adsorption on the metal-oxide shell surfaces.[60,63] Rhodium was found to promote the formation of formate ions due to the migration of atomic hydrogen to react with CO_2 molecule on the surface of metal oxide.[71] The pathway that CH_4 can be formed from formate species without CO being an intermediate and the reaction elementary steps can be briefly described as follows:[72]

$$CO_2 + H_2O \rightarrow HCOOH \quad (1)$$

$$HCOOH \rightarrow HCHO + 1/2O_2 \quad (2)$$

$$HCHO + H_2O \rightarrow CH_3OH + 1/2O_2 \quad (3)$$

$$CH_3OH \rightarrow CH_4 + 1/2O_2 \quad (4)$$

Here, CO can also be formed, but it forms to a lesser extent from the dissociation of formate species.[73,74] Although both pathways may occur simultaneously, it is expected that one process may dominate, depending on the experimental conditions. For example, the formate pathway may become significant after a sufficient amount of H_2 is produced, because formate can form easily in an H_2 environment. This could be the reason that CO is produced during the first 2 h and then is largely inhibited for Rh/Cr_2O_3 decorated GaN nanowires, as shown in Figure 3b. In either pathway, the effective adsorption of CO on Cr_2O_3 may facilitate its further reduction to methane.[62,65,75] It is worth mentioning that O_2 was also detected during the course of these experiments where the source of oxygen could be the combination of water oxidation and/or other reactions. The photoreduction rate of CO_2 into CO and CH_4 on GaN nanowires and Rh/Cr_2O_3-deocrated nanowires, respectively, were higher than previously reported nanostructured materials.[76−81] Moreover, the main products of CO and CH_4 on GaN and Rh/Cr_2O_3-deocrated wires increase linearly with illumination time. The nearly constant reduction rate of CO_2 to CH_4 and CO over 24 h suggests the stability of GaN nanowires during CO_2 photoreduction.

Further studies were also performed by promoting Pt nanoparticles on GaN nanowire surfaces. Figure 4 shows the

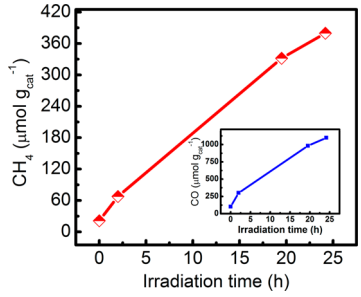

Figure 4. CH_4 evolution over Pt-decorated GaN nanowires as a function of illumination time. The inset shows CO generation on Pt-decorated nanowires over 24 h under illumination.

measured CH_4 evolution (~14.8 μmol g_{cat}^{-1} h^{-1}) over 24 h on Pt-decorated GaN nanowires, which is nearly 1 order of magnitude higher than that produced on bare GaN. The CO evolution rate, on the other hand, has not been significantly improved by promoting Pt nanoparticles, shown in the inset of Figure 4. Similarly, evolutions of both CO and CH_4 exhibit linear increase, indicating stable photocatalytic CO_2 reduction.

DOI: 10.1021/acscatal.5b00776
ACS Catal. 2015, 5, 5342−5348

Comparing with some previously reported Pt promoted nanomaterials, Pt-decorated GaN nanowires shows higher activity.[82−89] It is worth mentioning that the effective separation of hot carriers, together with the reduction of CO_2 activation barrier by Pt metal cocatalyst, may be the major reasons for this enhancement.[53] Besides activating the CO_2 molecule, efficient H_2 generation and adsorption on Pt nanoparticles could promote and accelerate CH_4 formation.[90−92] The available states on Pt have less energy than the GaN conduction band minimum, and therefore, photoexcited hot electrons can easily transfer to Pt metal. These electrons can be effectively involved in the multielectron CO_2 reduction process. It was previously reported that CO_2 can disassociate on Pt to form CO and O_2 at room temperature.[50] The reduction of CO_2 to CO by Pt-catalyzed TiO_2 was suggested to be a two-electron process,[7,55] wherein the elementary reaction steps are described as follows:

$$CO_2 + H^+ + e^- \rightarrow HCO_{2(ads)} \quad (5)$$

$$HCO_{2(ads)} + H^+ + e^- \rightarrow CO + H_2O \quad (6)$$

$$2H_2O + 2h^+ \rightarrow 2OH_{(ads)} + 2H^+ \quad (7)$$

$$2OH_{(ads)} \rightarrow 1/2O_2 + H_2O \quad (8)$$

In this process, holes can be provided simultaneously by GaN nanowires. Hence, the reaction is likely to occur close to the interface between GaN and Pt nanoparticles. CO can be adsorbed on Pt[93] and react further with atomic hydrogen to form methane:[7]

$$CO + 6e^- + 6H^+ \rightarrow CH_4 + H_2O \quad (9)$$

In this regard, the multielectron reduction could be the rate-determining step for CH_4 formation. On the other hand, the evolutions of CO on Pt-decorated nanowire and on as-grown nanowires are on the same order. This may indicate that electron-transfer rate is comparable to (or larger than) the kinetics limit of CO formation rate. For the case of Pt-decorated GaN, the diffusion of electrons to nanoparticles could be the rate-determining step due to the Coulomb repulsion induced by accumulated electrons on Pt nanoparticles.[94] Further investigation is required to determine the reaction pathway and the rate-determine step.

CONCLUSION

In summary, we have demonstrated the photocatalytic reduction of CO_2 on GaN nanowires, with CH_4 and CO being the major products. The reaction exhibits relatively high conversion rate and stability over 24 h. Promoting Rh/Cr_2O_3 core/shell nanoparticles showed an enhancement of the reaction rate and selectivity toward CH_4 over CO. It was also found that Pt nanoparticles could significantly enhance the activity of CO_2 reduction to CH_4. Future work includes the development of InGaN nanowire photocatalysts for the reduction of CO_2 into useful chemical fuels under visible light irradiation. The use of engineered nanostructured cocatalysts, together with variations of the surface charge properties of nanowires, to manipulate and control the CO_2 photoreduction pathways will also be investigated.

METHODS

S1. Molecular Beam Epitaxial (MBE) Growth. The vertically aligned GaN nanowires were grown on a low resistivity (<0.005 Ωcm) n-type Si(111) substrate by radio frequency plasma-assisted MBE under nitrogen-rich conditions without any foreign metal catalyst. Prior to loading into the MBE chamber, the Si(111) substrate was cleaned with acetone and methanol to remove any organic contaminants. Subsequently, Si substrate was immersed in 10% hydrofluoric acid (HF) to remove native oxide. Before the growth initiation, in situ oxide desorption was performed at ∼770 °C until the formation of a clean Si (111) 7 × 7 reconstructed surface was confirmed by reflection high-energy electron diffraction (RHEED). Thermal effusion cell was used as a source for Ga. Approximately one monolayer of a Ga seeding layer was deposited to promote the nucleation of the nanowires before growth initiation. Nitrogen ions were delivered from a radio frequency plasma source. The growth parameters include a substrate temperature of ∼750 °C, a nitrogen flow rate of 1.0 standard cubic centimeters per minute (sccm), a forward plasma power of ∼350 W, and a Ga beam equivalent pressure (BEP) of ∼6×10^{-8} Torr.

S2. Photodeposition of Cocatalyst. The deposition of Rh/Cr_2O_3 was carried out using a two-step photodeposition process. The advantage of this technique is that the metal particles are preferentially reduced on the reactive sites on the surface of the photocatalyst (i.e., GaN nanowires lateral nonpolar surfaces) by photogenerated electrons. First, GaN nanowire photocatalyst sample was placed in a Pyrex chamber. To deposit Rh particles, a 2 μL of 0.2 M sodium hexachlororhodate(III) (Na_3RhC_6, Sigma-Aldrich), 12 mL of CH_3OH (i.e., scavenger), and 60 mL of Milli-Q (∼18 MΩ) water were poured in the Pyrex chamber with quartz window. The cell was irradiated using 300 W xenon lamp (PerkinElmer, PE300BF) for 15 min after evacuation. Similarly, Cr_2O_3 deposition was followed with 2 μL of 0.2 M potassium chromate (K_2CrO_4, Sigma-Aldrich) as a precursor. The sample was then irradiated for 30 min. Pt nanoparticles photodeposition was carried out in the same manner as Rh. Four microliters of 1.5 M chloroplatinic acid hydrate solution was added to CH_3OH and water and illuminated for 30 min.

S3. Scanning Transmission Electron Microscopy (STEM). For STEM HAADF imaging, a Hitachi HD2700 Cs-corrected dedicated STEM was used with a cold field emission emitter operated at 200 kV and with an electron beam diameter of ∼0.1 nm.

S4. Photochemical CO_2 Reduction. The CO_2 reduction and product evaluation experiments were performed in an airtight gas circulation system (∼450 mL). The wafer-based GaN nanowires (area ∼3.5 cm^2) were carefully washed before putting at the bottom of the Pyrex reaction cell. The circulation system was first well evacuated and then filled with pure CO_2 until reaching a pressure of 80 kPa. Two milliliters of distilled water was then added into the reaction cell. The added water was vaporized under the illumination of a 300 W Xe lamp (ILC Tech, CERMAX LX-300), which was also used as the light source for the reaction. The products were measured by a gas chromatograph (GC-14B, Shimadzu) equipped with a flame ionization detector followed by hydrogenation reactor for CO evaluation. The absence of carbon residues on the samples was confirmed by control experiments. None of the reported products were detected without adding CO_2 reactant. In

DOI: 10.1021/acscatal.5b00776
ACS Catal. 2015, 5, 5342−5348

addition, $^{13}CO_2$ was used as reactant to further confirm that the source of C in CO and CH_4 was from CO_2 (Supporting Information S4).

■ ASSOCIATED CONTENT

Supporting Information

The Supporting Information is available free of charge on the ACS Publications website at DOI: 10.1021/acscatal.5b00776.

Description of the materials used in the experiments (PDF)

■ AUTHOR INFORMATION

Corresponding Author

*E-mail: zetian.mi@mcgill.ca. Phone: 1 514 398 7114.

Notes

The authors declare no competing financial interest.

■ ACKNOWLEDGMENTS

This work was supported by the Natural Sciences and Engineering Research Council of Canada and the Climate Change and Emissions Management (CCEMC) Corporation. B.A. acknowledges King Abdullah foreign scholarship program.

■ REFERENCES

(1) Tollefson, J. *Nature* **2011**, *473*, 134−134.
(2) Lewis, N. S.; Nocera, D. G. *Proc. Natl. Acad. Sci. U. S. A.* **2006**, *103*, 15729−15735.
(3) Smol, J. P. *Nature* **2012**, *483*, S12−S15.
(4) Pearson, P. N.; Palmer, M. R. *Nature* **2000**, *406*, 695−699.
(5) Inoue, T.; Fujishima, A.; Konishi, S.; Honda, K. *Nature* **1979**, *277*, 637−638.
(6) Serpone, N.; Borgarello, E.; Gratzel, M. *J. Chem. Soc., Chem. Commun.* **1984**, 342−344.
(7) Varghese, O. K.; Paulose, M.; LaTempa, T. J.; Grimes, C. A. *Nano Lett.* **2009**, *9*, 731−737.
(8) Habisreutinger, S. N.; Schmidt-Mende, L.; Stolarczyk, J. K. *Angew. Chem., Int. Ed.* **2013**, *52*, 7372−7408.
(9) Izumi, Y. *Coord. Chem. Rev.* **2013**, *257*, 171−186.
(10) Roy, S. C.; Varghese, O. K.; Paulose, M.; Grimes, C. A. *ACS Nano* **2010**, *4*, 1259−1278.
(11) Wang, S. B.; Lin, J. L.; Wang, X. C. *Phys. Chem. Chem. Phys.* **2014**, *16*, 14656−14660.
(12) Wang, S. B.; Ding, Z. X.; Wang, X. C. *Chem. Commun.* **2015**, *51*, 1517−1519.
(13) Koppenol, W. H.; Rush, J. D. *J. Phys. Chem.* **1987**, *91*, 4429−4430.
(14) Fujii, K.; Ohkawa, K. *Jpn. J. Appl. Phys. 2* **2005**, *44*, L909−L911.
(15) Beach, J. D.; Collins, R. T.; Turner, J. A. *J. Electrochem. Soc.* **2003**, *150*, A899−A904.
(16) Tran, P. D.; Wong, L. H.; Barber, J.; Loo, J. S. C. *Energy Environ. Sci.* **2012**, *5*, 5902−5918.
(17) Wang, C. J.; Thompson, R. L.; Baltrus, J.; Matranga, C. *J. Phys. Chem. Lett.* **2010**, *1*, 48−53.
(18) Yotsuhashi, S.; Deguchi, M.; Zenitani, Y.; Hinogami, R.; Hashiba, H.; Yamada, Y.; Ohkawa, K. *Appl. Phys. Exp.* **2011**, *4*, 117101.
(19) Yotsuhashi, S.; Deguchi, M.; Zenitani, Y.; Hinogami, R.; Hashiba, H.; Yamada, Y.; Ohkawa, K. *Jpn. J. Appl. Phys.* **2012**, *51*, 02BP07.
(20) Huygens, I. M.; Strubbe, K.; Gomes, W. P. *J. Electrochem. Soc.* **2000**, *147*, 1797−1802.
(21) Luo, W. J.; Liu, B.; Li, Z. S.; Xie, Z. L.; Chen, D. J.; Zou, Z. G.; Zhang, R. *Appl. Phys. Lett.* **2008**, *92*, 262110.
(22) AlOtaibi, B.; Nguyen, H. P. T.; Zhao, S.; Kibria, M. G.; Fan, S.; Mi, Z. *Nano Lett.* **2013**, *13*, 4356−4361.
(23) Caccamo, L.; Hartmann, J.; Fàbrega, C.; Estradé, S.; Lilienkamp, G.; Prades, J. D.; Hoffmann, M. W. G.; Ledig, J.; Wagner, A.; Wang, X.; Lopez-Conesa, L.; Peiró, F.; Rebled, J. M.; Wehmann, H.-H.; Daum, W.; Shen, H.; Waag, A. *ACS Appl. Mater. Interfaces* **2014**, *6*, 2235−2240.
(24) AlOtaibi, B.; Harati, M.; Fan, S.; Zhao, S.; Nguyen, H. P. T.; Kibria, M. G.; Mi, Z. *Nanotechnology* **2013**, *24*, 175401.
(25) Kibria, M. G.; Chowdhury, F. A.; Zhao, S.; AlOtaibi, B.; Trudeau, M. L.; Guo, H.; Mi, Z. *Nat. Commun.* **2015**, *6*, 6797.
(26) Ebaid, M.; Kang, J.-H.; Lim, S.-H.; Cho, Y.-H.; Ryu, S.-W. *RSC Adv.* **2015**, *5*, 23303−23310.
(27) Maeda, K.; Domen, K. *Chem. Mater.* **2010**, *22*, 612−623.
(28) Maeda, K.; Domen, K. *J. Phys. Chem. C* **2007**, *111*, 7851−7861.
(29) Wang, D. F.; Pierre, A.; Kibria, M. G.; Cui, K.; Han, X. G.; Bevan, K. H.; Guo, H.; Paradis, S.; Hakima, A. R.; Mi, Z. T. *Nano Lett.* **2011**, *11*, 2353−2357.
(30) Kibria, M. G.; Zhao, S.; Chowdhury, F. A.; Wang, Q.; Nguyen, H. P. T.; Trudeau, M. L.; Guo, H.; Mi, Z. *Nat. Commun.* **2014**, *5*, 3825.
(31) Anpo, M.; Chiba, K. *J. Mol. Catal.* **1992**, *74*, 207−212.
(32) Saladin, F.; Forss, L.; Kamber, I. *J. Chem. Soc., Chem. Commun.* **1995**, 533−534.
(33) Mori, K.; Yamashita, H.; Anpo, M. *RSC Adv.* **2012**, *2*, 3165−3172.
(34) Nguyen, H. P. T.; Zhang, S.; Cui, K.; Han, X.; Fathololoumi, S.; Couillard, M.; Botton, G. A.; Mi, Z. *Nano Lett.* **2011**, *11*, 1919−1924.
(35) Moustakas, T. D. T *Phys. Status Solidi A* **2013**, *210*, 169−174.
(36) Van de Walle, C. G.; Segev, D. *J. Appl. Phys.* **2007**, *101*, 081704.
(37) Liliental-Weber, Z.; Jasinski, J.; Zakharov, D. N. *Opto-Electron Rev.* **2004**, *12*, 339−346.
(38) Glas, F. *Phys. Rev. B* **2006**, *74*, 121302.
(39) Duan, X. F.; Niu, C. M.; Sahi, V.; Chen, J.; Parce, J. W.; Empedocles, S.; Goldman, J. L. *Nature* **2003**, *425*, 274−278.
(40) Fan, H. J.; Werner, P.; Zacharias, M. *Small* **2006**, *2*, 700−717.
(41) Zhao, S.; Kibria, M. G.; Wang, Q.; Nguyen, H. P. T.; Mi, Z. *Nanoscale* **2013**, *5*, 5283−5287.
(42) Van de Walle, C. G.; Stampfl, C.; Neugebauer, J. *J. Cryst. Growth* **1998**, *189-190*, 505−510.
(43) Gotz, W.; Johnson, N. M.; Chen, C.; Liu, H.; Kuo, C.; Imler, W. *Appl. Phys. Lett.* **1996**, *68*, 3144−3146.
(44) Schäfer, S.; Wyrzgol, S. A.; Lercher, J. A.; Stutzmann, M.; Sharp, I. D. *ChemCatChem* **2013**, *5*, 3224−3227.
(45) Yoshida, M.; Yamakata, A.; Takanabe, K.; Kubota, J.; Osawa, M.; Domen, K. *J. Am. Chem. Soc.* **2009**, *131*, 13218−13219.
(46) Tung, R. T. *Phys. Rev. B: Condens. Matter Mater. Phys.* **1992**, *45*, 13509−13523.
(47) Chen, X. B.; Li, C.; Gratzel, M.; Kostecki, R.; Mao, S. S. *Chem. Soc. Rev.* **2012**, *41*, 7909−7937.
(48) Kubacka, A.; Fernandez-Garcia, M.; Colon, G. *Chem. Rev.* **2012**, *112*, 1555−1614.
(49) Kibria, M. G.; Nguyen, H. P. T.; Cui, K.; Zhao, S.; Liu, D.; Guo, H.; Trudeau, M. L.; Paradis, S.; Hakima, A.-R.; Mi, Z. *ACS Nano* **2013**, *7*, 7886−7893.
(50) Tanaka, K.; White, J. M. *J. Phys. Chem.* **1982**, *86*, 3977−3980.
(51) Rasko, J. *Catal. Lett.* **1998**, *56*, 11−15.
(52) Erdohelyi, A.; Kocsis, M.; Bansagi, T.; Solymosi, F. *Acta. Chim. Hung.* **1982**, *111*, 591−605.
(53) Kamat, P. V. *J. Phys. Chem. Lett.* **2012**, *3*, 663−672.
(54) Foresi, J. S.; Moustakas, T. D. *Appl. Phys. Lett.* **1993**, *62*, 2859−2861.
(55) Tanaka, K.; Miyahara, K.; Toyoshima, I. *J. Phys. Chem.* **1984**, *88*, 3504−3508.
(56) Rasko, J.; Solymosi, F. *J. Phys. Chem.* **1994**, *98*, 7147−7152.
(57) Maeda, K.; Teramura, K.; Lu, D. L.; Takata, T.; Saito, N.; Inoue, Y.; Domen, K. *Nature* **2006**, *440*, 295−295.
(58) Maeda, K.; Teramura, K.; Saito, N.; Inoue, Y.; Domen, K. *Bull. Chem. Soc. Jpn.* **2007**, *80*, 1004−1010.
(59) Rostrupnielsen, J. R.; Hansen, J. H. B. *J. Catal.* **1993**, *144*, 38−49.

DOI: 10.1021/acscatal.5b00776
ACS Catal. 2015, 5, 5342−5348

(60) Sarusi, I.; Fodor, K.; Baan, K.; Oszko, A.; Potari, G.; Erdohelyi, A. *Catal. Today* **2011**, *171*, 132−139.
(61) Maeda, K.; Teramura, K.; Lu, D. L.; Saito, N.; Inoue, Y.; Domen, K. *J. Phys. Chem. C* **2007**, *111*, 7554−7560.
(62) Kuhlenbeck, H.; Xu, C.; Dillmann, B.; Hassel, M.; Adam, B.; Ehrlich, D.; Wohlrab, S.; Freund, H. J.; Ditzinger, U. A.; Neddermeyer, H.; Neuber, M.; Neumann, M. *Ber. Bunsen. Phys. Chem.* **1992**, *96*, 15−27.
(63) Solymosi, F.; Erdohelyi, A.; Kocsis, M. *J. Catal.* **1980**, *65*, 428−436.
(64) Rissmann, E. F.; Parry, J. M. *Catal. Lett.* **1992**, *16*, 159−164.
(65) Solymosi, F.; Tombacz, I. *Catal. Lett.* **1994**, *27*, 61−65.
(66) Kohno, Y.; Hayashi, H.; Takenaka, S.; Tanaka, T.; Funabiki, T.; Yoshida, S. *J. Photochem. Photobiol., A* **1999**, *126*, 117−123.
(67) Abee, M. W.; York, S. C.; Cox, D. F. *J. Phys. Chem. B* **2001**, *105*, 7755−7761.
(68) Park, J. N.; McFarland, E. W. *J. Catal.* **2009**, *266*, 92−97.
(69) Chen, Y. G.; Tomishige, K.; Yokoyama, K.; Fujimoto, K. *Appl. Catal., A* **1997**, *165*, 335−347.
(70) Galuszka, J. *Catal. Today* **1994**, *21*, 321−331.
(71) Solymosi, F.; Erdohelyi, A.; Bansagi, T. *J. Chem. Soc., Faraday Trans. 1* **1981**, *77*, 2645−2657.
(72) Aurianblajeni, B.; Halmann, M.; Manassen, J. *Sol. Energy* **1980**, *25*, 165−170.
(73) Arunajatesan, V.; Subramaniam, B.; Hutchenson, K. W.; Herkes, F. E. *Chem. Eng. Sci.* **2007**, *62*, 5062−5069.
(74) Goguet, A.; Meunier, F. C.; Tibiletti, D.; Breen, J. P.; Burch, R. *J. Phys. Chem. B* **2004**, *108*, 20240−20246.
(75) Elvins, O. C.; Nash, A. W. *Nature* **1926**, *118*, 154−154.
(76) Wang, W. N.; Park, J.; Biswas, P. *Catal. Sci. Technol.* **2011**, *1*, 593−600.
(77) Park, H. A.; Choi, J. H.; Choi, K. M.; Lee, D. K.; Kang, J. K. *J. Mater. Chem.* **2012**, *22*, 5304−5307.
(78) Lekse, J. W.; Underwood, M. K.; Lewis, J. P.; Matranga, C. *J. Phys. Chem. C* **2012**, *116*, 1865−1872.
(79) Zhou, Y.; Tian, Z. P.; Zhao, Z. Y.; Liu, Q.; Kou, J. H.; Chen, X. Y.; Gao, J.; Yan, S. C.; Zou, Z. G. *ACS Appl. Mater. Interfaces* **2011**, *3*, 3594−3601.
(80) Li, X. K.; Pan, H. Q.; Li, W.; Zhuang, Z. J. *Appl. Catal., A* **2012**, *413-414*, 103−108.
(81) Xie, Y. P.; Liu, G.; Yin, L. C.; Cheng, H. M. *J. Mater. Chem.* **2012**, *22*, 6746−6751.
(82) Pan, J.; Wu, X.; Wang, L. Z.; Liu, G.; Lu, G. Q.; Cheng, H. M. *Chem. Commun.* **2011**, *47*, 8361−8363.
(83) Guan, G. Q.; Kida, T.; Yoshida, A. *Appl. Catal., B* **2003**, *41*, 387−396.
(84) Li, P.; Ouyang, S. X.; Xi, G. C.; Kako, T.; Ye, J. H. *J. Phys. Chem. C* **2012**, *116*, 7621−7628.
(85) Zhang, N.; Ouyang, S. X.; Li, P.; Zhang, Y. J.; Xi, G. C.; Kako, T.; Ye, J. H. *Chem. Commun.* **2011**, *47*, 2041−2043.
(86) Zhang, N.; Ouyang, S. X.; Kako, T.; Ye, J. H. *Chem. Commun.* **2012**, *48*, 1269−1271.
(87) Liu, Q.; Zhou, Y.; Ma, Y.; Zou, Z. G. *RSC Adv.* **2012**, *2*, 3247−3250.
(88) Liu, Q.; Zhou, Y.; Tian, Z. P.; Chen, X. Y.; Gao, J.; Zou, Z. G. *J. Mater. Chem.* **2012**, *22*, 2033−2038.
(89) Wang, W. N.; An, W. J.; Ramalingam, B.; Mukherjee, S.; Niedzwiedzki, D. M.; Gangopadhyay, S.; Biswas, P. *J. Am. Chem. Soc.* **2012**, *134*, 11276−11281.
(90) Nikolic, B. Z.; Huang, H.; Gervasio, D.; Lin, A.; Fierro, C.; Adzic, R. R.; Yeager, E. B. *J. Electroanal. Chem. Interfacial Electrochem.* **1990**, *295*, 415−423.
(91) Marcos, M. L.; Gonzalezvelasco, J.; Vara, J. M.; Giordano, M. C.; Arvia, A. J. *J. Electroanal. Chem. Interfacial Electrochem.* **1989**, *270*, 205−224.
(92) Uner, D.; Oymak, M. M. *Catal. Today* **2012**, *181*, 82−88.
(93) Tanaka, K.; White, J. M. *J. Catal.* **1983**, *79*, 81−94.
(94) Amirav, L.; Alivisatos, A. P. *J. Am. Chem. Soc.* **2013**, *135*, 13049−13053.

DOI: 10.1021/acscatal.5b00776
ACS Catal. 2015, 5, 5342−5348